

# SUAS 2025 Design Report

Team Arrow  
Institute of Technology, Nirma University

**Abstract**—This paper presents the design methodology, mission strategy, and system validation of a UAS developed by a multidisciplinary team for the SUAS 2025 Competition. Under strict weight and volume constraints, the UAS is developed through an iterative, mission-optimized design process leveraging prior system experience to achieve autonomous flight, mapping, object detection, and payload delivery. Each subsystem is selected based on theoretical analysis and underwent rigorous testing before integration, achieving lightweight design, extended endurance, high-speed performance, and ease of transport. As a result, the *ARW1000* was successfully developed.

## I. ACKNOWLEDGEMENT

Our journey toward the SUAS competition has been an incredible experience, made possible through the crucial support of organizations as well as individuals beyond the development team. As we continue to work toward the competition, we remain deeply grateful to everyone who has contributed to our progress. We thank *Nirma University* for their comprehensive encouragement and a grant of approximately \$6,500, without which the project would not have been feasible. Access to laser cutting and soldering facilities provided by *Tinker's Lab* has significantly streamlined our workflow. We also acknowledge *M/s T-Motor* for the provision of ESCs, propellers and customized brushless motors as well as *M/s Carbon Matrix* for supplying aerospace grade carbon fiber composites and expert fabrication assistance.

We would like to express our heartfelt gratitude to our Faculty Advisors, Prof. Absar M. Lakdawala, Prof. Dhaval Shah and Prof. Chintan Patel for their invaluable technical guidance and thoughtful input throughout this project.

## II. COMPETITION STRATEGY

Our competition strategy is engineered to guarantee seamless execution of all mission tasks by combining reliability driven design with aggressive point maximization. We have designated total point accumulation as our primary objective, and every engineering decision is evaluated for its impact on system dependability under competition conditions. Only the vehicle's all-up weight and

the number of operators are treated as negotiable parameters every other parameter is fixed in to pursue full mark performance.

### A. Weight

The overall UAS weight represents a trade-off among subsystem selections and design choices. After evaluating multiple configurations, a robust structural design was finalized, optimizing the propulsion and power efficiency while maintaining high-speed capability. The integrated design ensures that the all-up weight remains within the target limit of 17.6 lbs with payload.

### B. Volume

The volume constraint brings critical challenges in the design process to ensure that the drone fits within the constraints of a personal item size (18" x 14" x 8"). Accomplishing this while maintaining functionality introduces design complexity. To address this challenge without compromise an innovative approach was adopted where detachable mechanical components were designed with a key focus on ease of assembly. The mounting scheme for all detachable components has been carefully designed to ensure quick assembly within 5 minutes of time limit.

### C. Number of Operators

To overcome false detection due to lower threshold for generalized dataset as well as change in environmental conditions, a third operator designated as the CS operator will focus on localizing the payload drop location based on captured images. This decision involves a point trade-off due to use of an additional operator. While the team is prepared for flight operations with two operators, the presence of the above challenges complicates the choice between employing two or three operators, necessitating a strategic balance between operational efficiency and scoring potential.

To overcome the limitations of generalized public datasets, we developed a synthetic dataset generator simulates airfield environments, producing annotations in XML, JSON, and YOLO-compatible TXT formats. YOLO[1] was selected

for object detection due to its real-time performance and high accuracy. It provided the best trade-off between speed and precision due to which alternatives like Faster R-CNN[2], SSD (Single Shot Multibox Detector), and DETR (DEtection TRansformer) were rejected. The choice between employing two or three operators will be determined by the performance outcomes of rigorous testing, ensuring that the strategy adopted maximizes both reliability and overall scoring effectiveness.

#### **D. Object Detection & Airdrop**

The team has adopted a full manual approach for object detection and localization to ensure high accuracy and avoid false positives caused by low-confidence detections from generic datasets. The survey field is pre-divided into multiple sections based on FOV of the camera. During the mission, the drone navigates to the center of each section and captures images. These images are then displayed in a custom-built GUI for operator analysis. A designated operator visually inspects each image, identifies targets and manually marks object positions within the frame. For localization, we implemented a custom algorithm that computes object positions by measuring pixel offsets from the image center and back-projecting them to ground coordinates using known drone altitude, GPS data, and camera field-of-view geometry. This controlled, operator-driven process ensures reliable classification and localization[3][4][5], aligning with mission objectives and minimizing the risk of point loss due to false detections or low-confidence thresholds. The winch mechanism is selected for the payload drop task due to its proven reliability and inherent safety of payload. A simple resistive braking[6] system is implemented to enable a controlled descent, thereby reducing electrical complexity and preventing free falls.

#### **E. Battery**

In compliance with battery transport regulations and mission requirement, six discrete cells, each with a capacity of 99.90 Wh, were selected for integration. To assemble these individual cells into a unified battery pack, a distinctive color-coded system was developed aiming for minimizing the risk of wiring errors and ensuring operational integrity.

#### **F. Mapping**

The mapping task demands high-resolution imagery, consistent coverage, and efficient post-processing. Mapping strategy is centered on optimizing both data acquisition and the stitching algorithm to ensure high-quality map outputs are produced within the strict time constraints of the competition. To meet these standards, the UAS operates at a speed of 13 m/s while 75% frontal and 70% side image overlap is maintained, conforming to standard photogrammetric requirements for reliable stitching and minimal reconstruction errors. Simultaneously, the flight path is autonomously generated using Mission Planner's AutoGrid feature, ensuring consistent and uniform end to end coverage across the mapping area.

Image capture is triggered by the flight controller at fixed distance synchronizing shutter actuation with the movement of UAS to maximize image sharpness and consistency. Concurrently, as soon as the first mapping image is captured, a backend process initiates parallel image downloads from the camera server to the ground station, thus minimizing latency and accelerating the post-processing workflow. Dedicated operator verifies the completeness and consistency of the received images in real time, ensuring no frames are missing or corrupted during transmission. The verified dataset is then processed using Image Composite Editor (ICE), chosen for its fast and accurate orthomosaic map generation, making it well-suited for time-sensitive mapping tasks.[7][8]

#### **G. Operational excellence**

Operational excellence is achieved by integrating strict safety measures with efficient operations. Conducting safe flight operations and thorough testing builds confidence, while optimizing the use of available equipment enhances performance without increasing input. This approach reflects strong commitment to operational excellence.

### **III. DESIGN STRATEGY**

Drone system architecture employs an iterative, concurrent engineering approach, where interdependent subsystems undergo parallelized component selection, integration and validation phases to optimize throughput. System is divided into subsystems levels for reducing complexity. An X configuration quadcopter was selected.

### A. Mechanical System

UAS is designed with the goals of ‘Design for Transport’ and stable flight operations. To attain maximum maneuverability while maintaining ideal stability in high wind conditions, a quadcopter with a 5 degree dihedral and deliberately elevated center of gravity is designed. Rotor arms are composed of twill weave 6K CFRP[9][10], which transitioned from a circular profile with OD 25mm and ID 23mm to a rectangular profile with 1.5 mm thickness at the ends. This design helps to retain torsional rigidity while reducing the number of components in assembly by avoiding incorporating the motor mount, thereby reducing the possibility of misalignment and vibrations caused by rapid changes in RPM, ESC is mounted inside the morphed rectangular cross-section to reduce complexity of mounting space and wiring. Z25 arm clamps are chosen due to their good strength, optimal weight and pin removal feature.

TABLE I: Drone Frame Dimensions

Feature	Dimension (in inch)
Wheelbase	37.46
Motor - motor distance	26.48
Height	14.28

The frame hub consists of two 2mm CFRP plates manufactured using a high pressure curing process which gave exceptional stiffness and strength to plates, reducing the vibration experienced by the flight controller. The top plate is designed to accommodate the PDB (Power Distribution Board) on top of it and under the battery plate improving accessibility along with reduction in frame hub size. Several design measures are taken into consideration including easily replaceable batteries, easy access to the flight controller, and sufficient clearance between plates for easy access to the electronics.

The team also included canopy to protect against gusty conditions and improve wake. It is designed for efficient flight operations up to a tilt angle of 30 degrees to the horizon[Fig. 10]. Carbon fiber sheet of 0.5mm thickness is vacuum moulded for the canopy[11][12] to save weight while maintaining ideal strength.

### B. Design for Transport

The design of UAS prioritizes rapid assembly and adhering to dimensional constraints equivalent to personal-item size. Central to this design is

a modular structural framework that minimizes complexity.

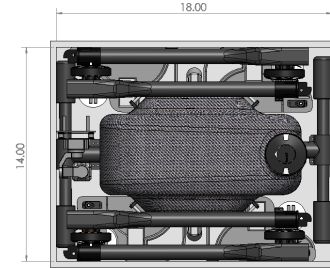


Fig. 1: ARW1000 Disassembled state (18" x 14" x 8")

The Z25 arm mounts are selected as removal of its pin-lock results in the disassembly of the arm rods from the drone frame. The dual T-type landing gear, secured by two bolts, is engineered to minimize assembly time while providing reliable ground contact. The landing clamp has been optimized to accommodate the landing gear and is designed to fit within the available space beneath the drone when stowed in its container. The modular design of the payload drop mechanism enables straightforward installation via a single bolt mounting under the bottom plate, thereby streamlining the overall system integration. The battery, camera, and canopy are optimized for rapid integration via wing bolt.



Fig. 2: Isometric view of ARW1000

### C. Propulsion System

Propulsion system is engineered to exceed a thrust-to-weight ratio of 3, while maintaining a hover throttle threshold below 65% under worst case aerodynamic loading. Through parametric optimization using manual 3D vector field analysis, power efficiency and propeller size drove selection of the T-Motor MN6007 II 320KV brushless motor paired with T-Motor NS22x6.6" propeller, supported by T-Motor Alpha 60A ESCs to accommodate peak transient current of 58A per

motor while ensuring thermal headroom to sustain high-thrust and switching operations. To reduce power consumption while maintaining propulsion performance and weight, an innovative motor alloy stator winding design has been implemented by substituting traditional copper windings with silver windings[Fig. 3]. This modification yields an average current reduction of 15% at equivalent thrust level, thereby decreasing the overall power consumption. This reduction is critical for ensuring that the UAS's all-up weight remains within the specified weight limit. Solid-State Lithium-Ion[13] battery of 27000mAH consisting of 6 cells leverages a flight time of nearly 33 minutes under extreme conditions.

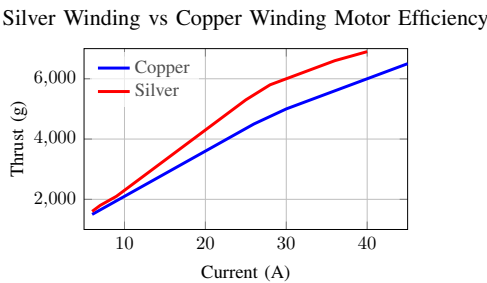


Fig. 3: Comparison of thrust for copper and silver wended MN6007-II 320KV motor.

#### D. Avionics System

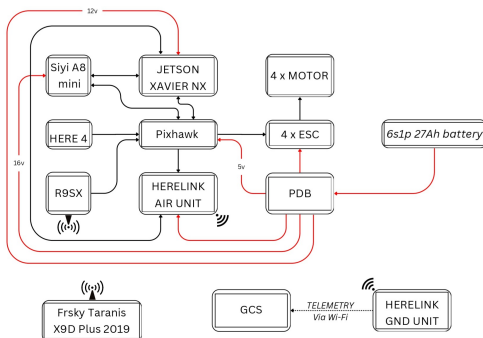


Fig. 4: Block Diagram of the UAS

1) **Autopilot:** A Pixhawk Cube orange+ with a mini carrier board controls autonomous flight for ARW1000, leveraging extensive expertise with the Pixhawk flight controllers and the benefits of open-source interfacing. Despite the computational load from running multiple algorithms, the system sustains a stable performance with a higher loop rate capacity. For precise navigation and achieving centimeter-level accuracy necessitates use of Here4 GPS, integrated via the CAN

protocol, which enables redundant communication under magnetic interference. The internal compass of the pixhawk exhibits instability under EMI[14] from adjacent avionics . To ensure robust heading accuracy, compass of Here4 is designated as the UAS's primary heading reference.

2) **Communication System:** Flight environment and operating region are key factors in selecting the communication system. Based on the team's prior experience with Herelink, its availability and proven reliability in longer range performance provides a data rate of 1500 kbps at a range of 1 Miles[Fig. 5]. Herelink system provides dual communication link for telemetry data and for high-definition video transmission in a single integrated module thus minimizes the mounting space requirements and simplifies wiring, making it a highly efficient choice for the system. H.265 video encoding chosen over H.264 for enabling improved compression efficiency of higher resolution images.

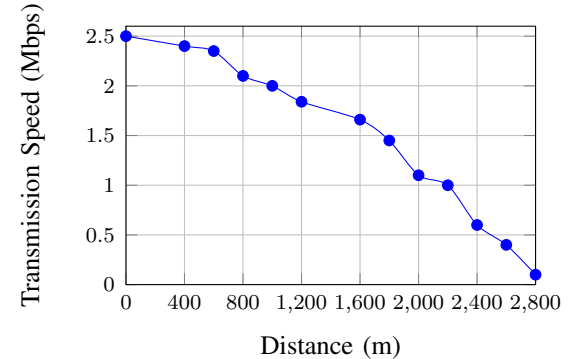


Fig. 5: Transmission speed v/s distance

Rather than relying on the Herelink's built-in radio link, we opted to pair the R9SX module with the Taranis X9D R9M. This decision was driven by the Taranis X9D's superior throttle control and enhanced stick response, which collectively offer a more refined pilot input shaping.

#### E. Imaging and Object Detection & Localization System

The imaging system is designed to meet operational requirements, ensuring reliable aerial data acquisition. These requirements include minimizing motion blur, reducing camera weight, achieving high-resolution images for mapping and object detection and enabling real-time data transfer. The system should also be integrated with

flight controllers, to maintain image stability during flight, and support efficient data processing for autonomous mission tasks. The SIYI A8 Mini was selected for its compact and lightweight design and cost efficiency ensuring optimal performance without compromising image quality.

It offers several advantages, including its internet protocol support making it compatible with communication system. It integrates smoothly with the flight controller and allows real time gimbal control, location-synchronized shutter activation and adaptive region of interest selection enhancing automated data acquisition. Camera features a global shutter that eliminates rolling distortion, crucial for photogrammetry or orthomosaic map generation and target recognition. The wider FOV covers the more object detection field from a certain altitude. However, compared to other cameras, the SIYI A8 Mini is limited to 4K resolution, which may lead to slight reductions in image quality and a lower GSD when generating maps. Despite this balance of performance, size, cost and functionality makes it an excellent choice.

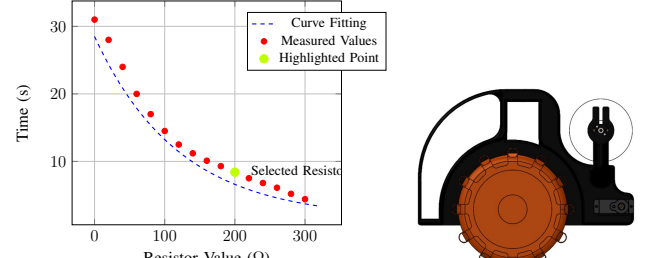
#### F. Airdrop Mechanism

A DC motorized winch mechanism has been engineered for precise payload deployment. The winch assembly is fabricated using 3D printed PETG material[15]. The winch wheel is actuated by a designated Emax ES08A servo motor in conjunction with an elastic strap, ensuring accurate and reliable control of the release process. The system is capable of autonomous deployment via the flight controller, while also allowing manual actuation by either the safety pilot or ground control station operator. A 98 feet length of nylon thread, secured to the payload via a hook, facilitates secure post-deployment retrieval. N20 1000 rpm DC motor, integrated with  $200\ \Omega$  resistor regulates the descent speed of the payload[Fig. 6a].

## IV. TESTING STRATEGY

### A. Vibration Testing & Notch Filter Tuning

To mitigate vibrational disturbances induced by motor and propeller rotation, dual damping strategies are employed. Mechanically, the flight controller is mounted on a dedicated vibration damper to attenuate vibrations. However, high-frequency vibrations in the airframe caused excessive movement of the flight controller on the damper, exacerbating vibrational issues. After extensive experimentation with various damping



(a) Time vs Resistor Value Characteristics (b) AirDrop Mechanism

Fig. 6: System characterization and deployment:  
(a) Time vs Resistor Value, (b) AirDrop Mechanism

configurations, a hard-mounted solution using silicon pads was adopted to enhance vibration attenuation. Configuring Software-based adaptive notch filters suppress resonant frequencies induced by propeller-arm interactions[FIG. 11]. Notch filters are configured with a trade-off between phase lag and the computational capacity of the autopilot system.

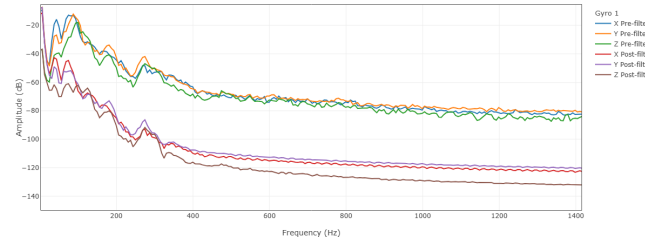


Fig. 7: UAS's Notch Frequencies

### B. Control System Testing

To ensure UAS maintains desired attitude under dynamic aerodynamic loading during the mission, precise tuning of the PID control[16][17][18] is necessary. The proportional, integral, and derivative gains are tuned via Autotune and Manual tune through iterative flight-test cycles, with help of time-domain and frequency-domain graphs to further validate stability margins under turbulent conditions [Fig. 8].

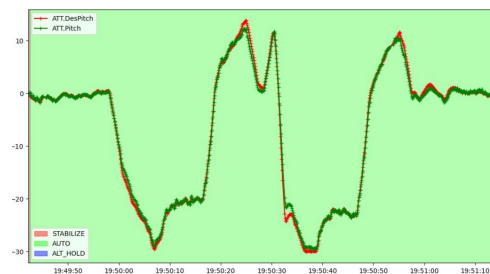


Fig. 8: Actual v/s Desired pitch at 20m/s Speed

Additionally, barometer compensation is done to enhance PIDs under aerodynamic loading and voltage scaling is performed to compensate for voltage surges occurring during in flight maneuvers.

### C. PDB Testing

To validate performance of the Power Distribution Board, it was subjected to tests beyond its standard operating range. It was tested at 75% throttle for 10 minutes, where temperature did not exceed safe operational limits. Additionally, to simulate worst-case scenarios with abrupt current spikes, the PDB was tested at 95% throttle for 35 seconds. In both tests, the measured temperature remained below 55°C and the vias successfully withstood the transient current surges, confirming its robust performance under dynamic load conditions.[19]

### D. Mechanical Testing

**1) Software Testing:** Various computational tests were performed to analyse and validate the design of the UAS. Aerodynamic characteristics and flow behaviours were analysed using CFD in Ansys Fluent leading to evaluation of drag and wake generation. Static and Dynamic structural analysis such as Modal analysis were performed to study the design under loaded conditions, which was performed using ANSYS 2024R1® and Fusion360. Incremental design changes were carried out over the results of such tests during development leading to the final mechanical design of the UAS.

Static structural studies involved application of thrust load and forces experienced during landing to analyse the stresses and deformation of the frame.

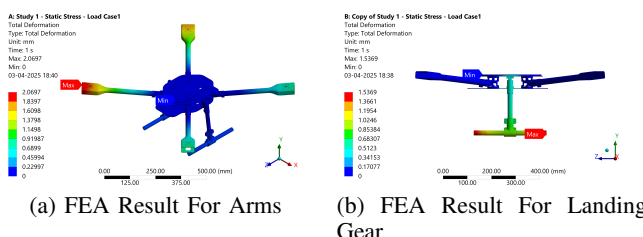


Fig. 9: FEA Simulation of Total Deformation Under Various Static Loads

The results showed a safety factor of 3.35 with maximum stress of 292.51 Mpa at deformation of 2.07 mm[Fig. 9] considering the thrust forces

during a maneuver. For a rough landing at forces 10 times greater than the weight was applied for which safety factor of 1.44 was achieved [Fig. 9b]. Modal analysis[20] led to the natural frequencies as shown in the [Table. II] When compared with the vibrational frequencies of the motors at maximum rpm i.e 5124 with its corresponding frequency 85.4 Hz, no interference was observed.

TABLE II: Mode Frequencies

Mode	Frequency (Hz)
1	93.501
2	129.19
3	157.02
4	158.26
5	165.59
6	177.23

Explicit Dynamics simulation was also performed to study a structure during a rough landing. The result showed that no critical components except the parts with high stress concentration such as T-clamp and TPU feet were damaged. CFD analysis[Fig. 10] was performed using SST k- $\omega$  model at different attitudes during hover as well as pitch attitudes with wind speed of 15m/s and the ground speed of UAS was assumed to be 25 m/s.[21]

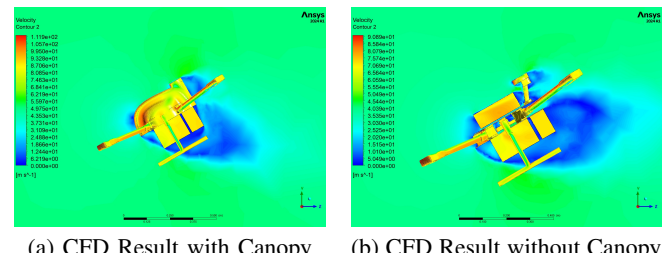


Fig. 10: Comparison of CFD simulation results

TABLE III: Drag Forces Comparison (in Newton)

UAS State	With Canopy	Without Canopy
Hover	17.66	18.13
Pitch (25 m/s)	55.86	57.18
Side	10.36	10.11

The computational testing led to many changes in the design leading to the final UAS. The CFD analysis helped in understanding the wake effects of the UAS and thus the flow around the drone was optimized further by inclusion of the canopy. Structural studies helped to validate durability and strength of the UAS, confirming a high safety factor which allows survival during a crash event or delaying effects of fatigue loading on the frame.

## REFERENCES

- [1] T. Panboonyuen, S. Thongbai, W. Wongweeranimit, P. Santiamnont, K. Suphan, and C. Charoenphon, "Object detection of road assets using transformer-based yolox with feature pyramid decoder on thai highway panorama," *Information*, vol. 13, p. 5, 12 2021, DOI: 10.3390/info13010005.
- [2] Y. Qian, H. Zheng, D. He, Z. Zhang, and Z. Zhang, "R-cnn object detection inference with deep learning accelerator," in *2018 IEEE/CIC International Conference on Communications in China (ICCC Workshops)*, 2018, pp. 297–302, DOI: 10.1109/ICCCChinaW.2018.8674519.
- [3] J. Liao, Y. Piao, s. Jinhe, G. Cai, X. Huang, L. Chen, Z. Huang, and Y. Wu, "Unsupervised cluster guided object detection in aerial images," *IEEE Journal of Selected Topics in Applied Earth Observations and Remote Sensing*, vol. 14, pp. 1–1, 01 2021, DOI: 10.1109/JSTARS.2021.3122152.
- [4] M. Nieuwenhuisen, D. Droschel, M. Beul, and S. Behnke, "Autonomous navigation for micro aerial vehicles in complex gnss-denied environments," *Journal of Intelligent and Robotic Systems*, 12 2016, DOI: 10.1007/s10846-015-0274-3.
- [5] M. Belhor, A. Savard, A. Fleury, P. Sondi, and V. Loscri, "Enhanced rf-based 3d uav outdoor geolocation: from trilateration to machine learning approaches," in *2024 IEEE 27th International Symposium on Real-Time Distributed Computing (ISORC)*, 2024, pp. 1–8, DOI: 10.1109/ISORC61049.2024.1055131.
- [6] S. Zarabian, Y. M. Amani, and S. Elsaia, "Experimental dynamic braking with energy storage and power generation capability for maritime industry," in *2018 IEEE Power & Energy Society General Meeting (PESGM)*, 2018, pp. 1–5, DOI: 10.1109/PESGM.2018.8586062.
- [7] S. Wang, Z. Guo, and Y. Liu, "An image matching method based on sift feature extraction and flann search algorithm improvement," *Journal of Physics: Conference Series*, vol. 2037, p. 012122, 09 2021, DOI: 10.1088/1742-6596/2037/1/012122.
- [8] S. Toki, S. Slack, and C. Coopmans, "Image quality assessment of uav simulator imagery based on different orthomosaic maps," 06 2024, pp. 923–928, DOI: 10.1109/ICUAS60882.2024.10556972.
- [9] C. Dong, J. Zhou, X. Ji, Y. Yin, and X. Shen, "Study of the curing process of carbon fiber reinforced resin matrix composites in autoclave processing," *Procedia Manufacturing*, vol. 37, pp. 450–458, 01 2019, DOI: 10.1016/j.promfg.2019.12.073.
- [10] P. Alam, D. Mamalis, C. Robert, C. Floreani, and C. O'Bradaigh, "The fatigue of carbon fibre reinforced plastics - a review," *Composites Part B: Engineering*, vol. 166, 02 2019, DOI: 10.1016/j.compositesb.2019.02.016.
- [11] K. Vallons, A. Behaeghe, S. Lomov, and I. Verpoest, "Impact and post-impact properties of a carbon fibre non-crimp fabric and a twill weave composite," *Composites Part A: Applied Science and Manufacturing*, vol. 41, pp. 1019–1026, 08 2010, DOI: 10.1016/j.compositesa.2010.04.008.
- [12] H. Koushyar, S. Alavi-Soltani, B. Minaie, and M. Violette, "Effects of variation in autoclave pressure, temperature, and vacuum-application time on porosity and mechanical properties of a carbon fiber/epoxy composite," *Journal of Composite Materials*, vol. 46, pp. 1985–2004, 08 2012, DOI: 10.1177/0021998311429618.
- [13] W. S. Khan and M. Darwish, "Advancing electric vehicle technologies: A comparative analysis of lithium-ion and emerging solid-state battery systems," in *2024 59th International Universities Power Engineering Conference (UPEC)*, 2024, pp. 1–5, DOI: 10.1109/UPEC61344.2024.10892478.
- [14] K. Watanabe, M. Aoi, M. Komatsu, S. Tanaka, and M. Nagata, "Measurements of electromagnetic emission nearby a compact drone," in *2021 Asia-Pacific International Symposium on Electromagnetic Compatibility (APEMC)*, 2021, pp. 1–4, DOI: 10.1109/APEMC49932.2021.9597146.
- [15] A. Economides, M. Islam, and K. Baxevanakis, "Additively manufactured carbon fibre petg composites: Effect of print parameters on mechanical properties," *Polymers*, vol. 16, p. 3336, 11 2024, DOI: 10.3390/polym16233336.
- [16] S. Kamni, A. Bertout, E. Grolleau, G. Hattenberger, and Y. Ouhammou, "Easing the tuning of drone autopilots through a model-based framework," *Journal of Computer Languages*, vol. 77, p. 101240, 2023, DOI: 10.1016/j.cola.2023.101240. [Online]. Available: <https://www.sciencedirect.com/science/article/pii/S2590118423000503>
- [17] A. Waheed, Z. Toor, M. M. Quamar, and S. Javaid, "Advancing drone autonomy: A comprehensive framework for agile controller design in quadcopters," *Transportation Research Procedia*, vol. 84, pp. 487–494, 2025, smart Mobility and Logistics Ecosystems. [Online]. Available: <https://www.sciencedirect.com/science/article/pii/S2352146525001486>
- [18] E. Yazid, M. Garratt, and F. Santoso, "Position control of a quadcopter drone using evolutionary algorithms-based self-tuning for first-order takagi-sugeno-kang fuzzy logic autopilots," *Applied Soft Computing*, vol. 78, pp. 373–392, 2019, DOI: 10.1016/j.asoc.2019.02.023. [Online]. Available: <https://www.sciencedirect.com/science/article/pii/S1568494619300833>
- [19] Y. Shen, H. Wang, F. Blaabjerg, H. Zhao, and T. Long, "Thermal modeling and design optimization of pcb vias and pads," *IEEE Transactions on Power Electronics*, vol. 35, no. 1, pp. 882–900, 2020, DOI: 10.1109/TPEL.2019.2915029.
- [20] F. Ahmad, P. Kumar, P. Patil, and V. Kumar, "Fea based frequency analysis of unmanned aerial vehicle (uav)," *Materials Today: Proceedings*, vol. 46, 02 2021, DOI: 10.1016/j.matpr.2020.12.740.
- [21] H. G. Parra P., V. D. Angulo M., and E. E. Gaona G., "Cfd analysis of two and four blades for multirotor unmanned aerial vehicle," in *2018 IEEE 2nd Colombian Conference on Robotics and Automation (CCRA)*, 2018, pp. 1–6, DOI: 10.1109/CCRA.2018.8588130.

APPENDIX A  
TEST PLAN AND RESULTS

Project management is optimized by segmenting the schedule into the following timeline.

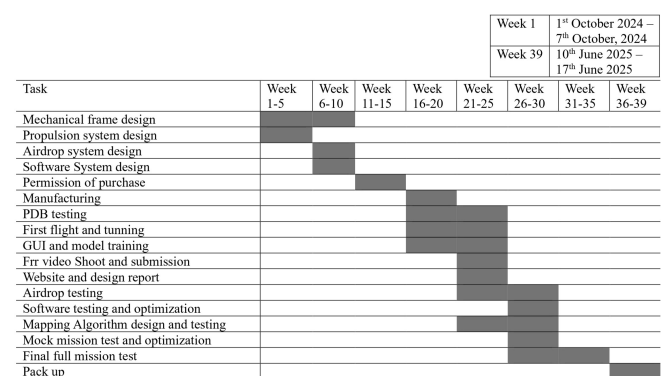


Fig. 11: Team's timeline for the SUAS'25

## APPENDIX B CAMERA SELECTION

The camera selection was driven by mission constraints such as field of view, resolution, weight, interface compatibility, shutter type, and overall system integration. The team initially considered the ADTi Surveyor V3. To meet real-time processing and stabilization needs without external hardware, the team selected the SIYI A8 Mini with a global shutter and Ethernet interface, supporting low-latency ground-based computation. Alternatives like the Sony Alpha 6000 (24.3 MP APS-C sensor) were dismissed. Arducam modules offered lightweight options but were limited by rolling shutter artifacts and synchronization issues, making them unsuitable for high-speed aerial imaging.

TABLE IV: Camera Selection Comparison

Camera	Resolu-	Shutter	Weight	Gimbal	Sel.
	tion	Type			
ADTi Surveyor V3	6000 x 4000	Global	108g	Yes	N
SIYI A8 Mini	4K (Video)	Global	100g	No	Y
Sony Alpha 6000 (24.3 MP)	6000 x 4000	Electronic / Mechanical	~344g	Yes	N

## APPENDIX C MAPPING TESTING

To validate the mapping workflow, the team selected Microsoft Image Composite Editor (ICE) due to its efficient orthomosaic stitching algorithms and rapid processing time, which align with the SUAS competition's time-constrained deliverables. Testing involved executing multiple autonomous mapping flights using grid missions generated via the AutoGrid tool in Mission Planner. Images were captured using the SIYI A8 Mini camera with a trigger-by-distance setup and transmitted images in real time to the ground station through a camera server. The captured datasets were imported into ICE to analyze stitching quality and generation time across various altitudes. Results showed that ICE consistently produced accurate orthomosaics with minimal artifacts, and

average map generation time was within 4.5 minutes for standard mission validating the suitability of this software-camera combination. The test environment consisted of clear outdoor conditions, ensuring optimal image quality.

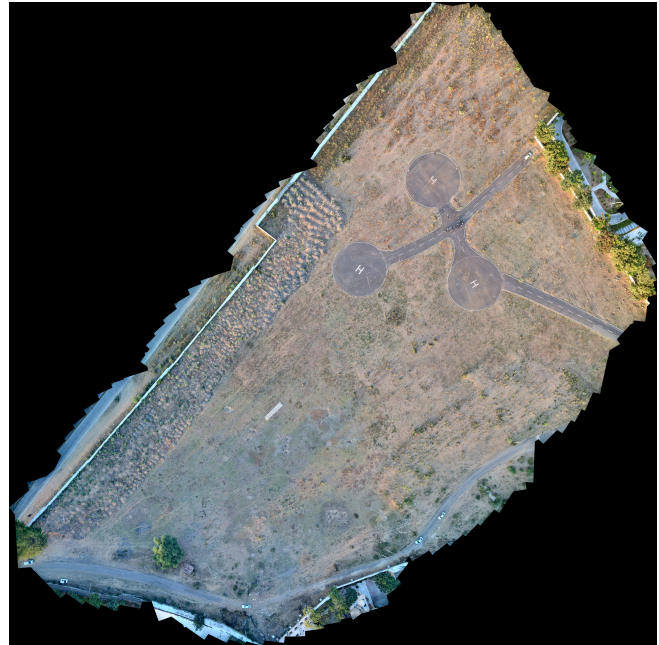


Fig. 12: Sample Mapped Area of 340m x 140m

## APPENDIX D OBJECT DETECTION ALGORITHM TESTING

The team explored multiple approaches for implementing a robust object detection algorithm, including training a YOLO-based detector, fine tuning large language models (LLMs) for visual grounding and experimenting with region-based (R-CNN) and transformer-based (DETR) models. Initial consideration was given to training on real world datasets; however, due to the generalized nature of SUAS targets and the unavailability of consistent real-world imagery for all object classes, this approach proved infeasible. To address data scarcity, the team developed a synthetic data generation pipeline that programmatically augmented object instances into aerial background images to simulate realistic scenarios. Fine tuning transformer-based and LLM-driven models led to unreliable detections and required significant computational resources, making them unsuitable under project constraints. Consequently, the team adopted the YOLO architecture for its balance of speed, accuracy, and inference efficiency. Extensive testing demonstrated its high reliability in detecting SUAS-relevant classes (e.g., stop signs, vehicles, sports balls) in both synthetic and limited

real imagery, making it the optimal choice for deployment.



Fig. 13: Model Confidence score

## APPENDIX E FUNCTIONAL AND SIMULATION TESTING

All system functionalities are initially validated within a virtual environment using Mission Planner's Software-in-the-Loop (SITL) simulation, ensuring safe and repeatable testing of core logic and mission scripts. Functional testing encompassed both unit-level and system-level evaluations. Individual modules—such as autonomous mission execution, camera triggering, real-time image downloading, and communication with the companion computer—were first tested in isolation within SITL to ensure robustness and error handling. Following successful simulation, hardware-in-the-loop functional testing was conducted on the physical drone platform to validate real-time behavior and integration with Mission Planner and onboard systems. Once verified, all modules were integrated, and comprehensive system-level testing was performed under controlled flight scenarios to ensure seamless operation across navigation, imaging, and data-handling subsystems. This iterative simulation-to-real workflow minimized risk and improved overall system reliability.

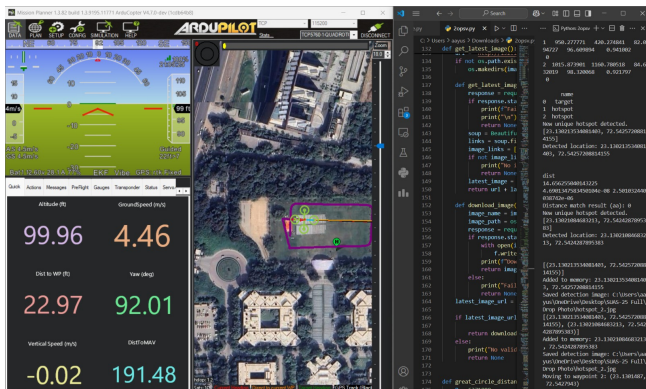


Fig. 14: Simulation of the Code for SUAS 2025

## **APPENDIX F**

# **DISCREPANCY IN ENVIRONMENTAL CONDITION**

One of the main concerns was addressing the difference in environmental conditions between the testing site and the competition venue. The competition site featured cooler temperatures and frequent gusty winds, unlike the more stable conditions at the testing location. To mitigate this discrepancy, several tests were conducted during early morning hours to simulate lower temperature conditions. Additionally, the drone was tested at multiple locations to evaluate its performance and adaptability under varying wind gust scenarios.

## APPENDIX G

# SOFTWARE USED

A range of industry-standard software tools was essential throughout the design, simulation, and testing phases. These specialized packages helped ensure precision, efficiency and reliability by enabling us to model the physical structure, simulate performance before building, program flight missions, design custom electronics, and optimize the power system. Software tools used during the entire development process are key factors in the development of ARW1000.

#### A. Solidworks (CAD Modelling)

Solidworks is a 3D Computer-Aided Design (CAD) design software which was extensively utilised for create detailed 3D model of the UAV airframe, internal structure and individual sub-assemblies. It enables the team to visualize the component placement and configuration. The software was also used to create parts for 3D printing of custom part.

#### *B. Fusion 360 (Pre-processing for Analysis)*

Fusion360 is a comprehensive 3D design and modelling tool which played a key role for pre-processing in structural analysis. The smooth design workflow, easy-to-use interface and large material library makes it a compelling choice for assigning materials, adding loads and constraints to model, which can be directly imported to ANSYS Workbench for solving. Fusion360's easier lofting and modelling was used to design the canopy of the UAS.

### C. ANSYS 2024R1® (Analysis and Results)

The vast and powerful engineering simulation software suite plays a crucial role for analysing and simulating the drone's design integrity before building physical prototypes. ANSYS 2024R1® Mechanical provides extensive solving and post-processing capabilities for Finite Element Analysis (FEA), which assesses the operational demands of the airframe. ANSYS Fluent module was used to perform Computational Fluid Dynamics (CFD) simulations to analyse the aerodynamic characteristics, helping to minimize drag and evaluating the airflow around the UAS.

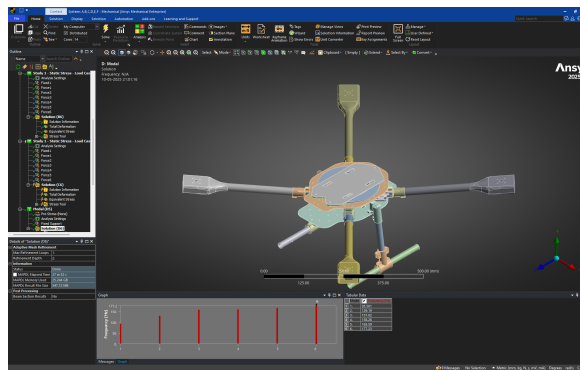


Fig. 15: Modal Analysis in Ansys 2024R1®

### D. Mission Planner (Mission Planning and Configuration)

Mission planner is chosen as the ground control station on the basis of customizability and experience of the team with this software. During test flights, it provided real-time monitoring of critical telemetry data and was subsequently used for detailed post-flight log analysis to fine-tune performance and troubleshoot any issues.

### E. Altium (PCB/PDB Designing)

This specialized electronic design automation (EDA) software is used for the complete lifecycle of custom printed circuit board (PCB) development for the drone.

This included capturing electronic schematics for various subsystems, performing detailed PCB layout with considerations for component placement and signal integrity, and generating the Gerber files required for board manufacturing. It enabled the creation of compact, reliable, and application-specific electronic boards tailored to the drone's requirements.

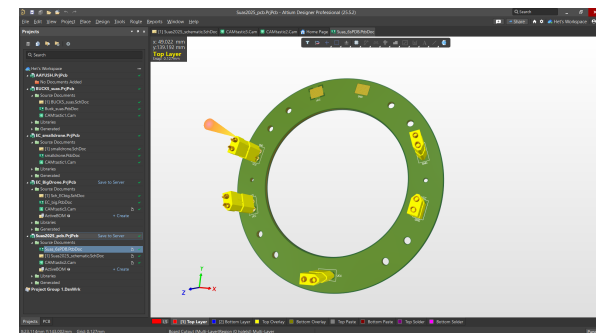
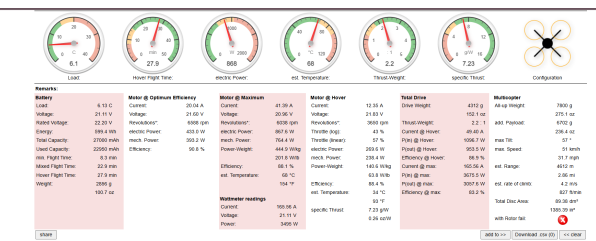


Fig. 16: PDB Designing in Altium

### F. Ecalc (Power and Propulsion System Design)

This online calculation and simulation tool is vital for designing and optimizing the drone's electric powertrain. By inputting various component specifications like motors, propellers, batteries, ESCs and frame size, E-Calc helped predict key performance metrics such as thrust, flight time, current draw, and overall efficiency. This allowed the team to select appropriately matched components, ensure they operated within safe limits, and design a power system that met the project's endurance and performance goals.



**TABLE V: Autopilot Flight Summary**

<b>Parameter</b>	<b>Value</b>
Total number of flights	348
Total number of manual flights	121
Total number of autonomous flights	227
Total waypoint attempted	2,270
Number of waypoint hits (considering 25ft error)	2,270
Total hours of flights taken	70
Number of flights aborted due to errors	35
Number of flights with fully loaded weight	90

Each flight was meticulously documented, capturing the success ratio and observed anomalies, thereby enabling a data driven and scientific approach for improvement. The table below summarizes the flight test overview undertaken during the development of ARW1000.

### *B. Airdrop Performance*

Winch mechanism used for air drop underwent rigorous testing independently developed from main design ensuring secure drop within desired radius of 25 feet. A key part of these tests involved using different resistor values in the winch mechanism and note time taken for the same, from a height of 100 feet. Recorded data proves reliability, precision and efficiency of winch mechanism, the tested system was then fitted to the main design.

**TABLE VI: Airdrop Operation Summary**

<b>Parameter</b>	<b>Value</b>
Number of airdrops performed	117
Mean accuracy of drop (in ft)	12
Mean time to complete the drop (in s)	11
Success rate (in %)	96.66
Accuracy of 90th percentile drop (in ft)	7

### *C. Full Mission Performance*

Recreating dummy missions and simulating the maximum possible range of conditions rigorously tests all scenarios the team may encounter during the mission.

**TABLE VII: Full Mission Execution Summary**

<b>Parameter</b>	<b>Value</b>
Total number of full mission flights	14
Total number of objects placed	58
Total number of objects detected	56
Successfull detection rate(2 operator)	96.93
Total number of drops performed	55
Number of successful drops (25ft error)	53
90th percentile drop (ft)	9
Average mission time to complete the mission (in min)	29.3

Addressing anomalies identified during mission testing enhances system reliability and builds confidence. Continuous testing of the complete mission cycle contributes to the team's consistent operational excellence. Below is the recorded data from full mission testing.

## **APPENDIX I WEBSITE**

The team also created a dedicated website ([link: www.teamarrow.in](http://www.teamarrow.in)) featuring a special SUAS competition section, where various technical blogs are presented with engaging visual enhancements.